Available online www.jocpr.com

Journal of Chemical and Pharmaceutical Research, 2014, 6(3):1187-1194

Research Article

ISSN : 0975-7384
CODEN(USA) : JCPRC5

Induced-fit docking and virtual screening for 8-hydroxy-3-methoxy-5H-pyrido [2,1-c] pyrazin-5-one derivatives as inducible nitric oxide synthase inhibitors

Hua-Jun Luo[1], Jun-Zhi Wang[1], Nian-Yu Huang[1], Wei-Qiao Deng[2] and Kun Zou[1]*

[1]*Hubei Key Laboratory of Natural Products Research and Development, College of Biology & Pharmacy, China Three Gorges University, Yichang, China*
[2]*Dalian Institute of Chemical Physics, Chinese Academy of Sciences, Dalian, China*

ABSTRACT

*8-Hydroxy-3-methoxy-5H-pyrido [2, 1-c] pyrazin-5-one (compound **1**) isolated from Solanum cathayanum was identified as an inducible nitric oxide synthase (iNOS) inhibitor with IC_{50} value 30 μM. Induced-fit docking (IFD) was performed to investigate the interaction mechanism between compound **1** and iNOS. The Glide Gscore and IFD score of compound **1** are –6.99 and –766.90, respectively. Hydroxyl group of compound **1** has hydrogen bond interaction with cofactor iron protoporphyrin. The derivatives of compound **1** as novel iNOS inhibitors were designed using combinatorial virtual screening technology. The IFD scores of top 5 compounds range from –769.00 to –775.32. The selected top compounds have more binding sites than compound **1**, and interact with both iron protoporphyrin and key residues such as Gln257, Tyr341, Met368, and Glu371.*

Keywords: iNOS inhibitor; induced-fit docking; virtual screening

---

INTRODUCTION

Nitric oxide synthase (NOS) catalyzes the production of nitric oxide (NO), which is a reactive free radical molecule with an important role in various physiological processes, including modulation of inflammatory responses and regulation of cardiovascular system [1-4]. Three major isoforms of NOS have been identified in mammals: neuronal NOS (nNOS), endothelial NOS (eNOS) and inducible NOS (iNOS) [5]. Neuronal NOS (nNOS) and endothelial NOS (eNOS) are constitutively expressed under non-inflammatory conditions, and their activity is tightly regulated by Ca^{2+}-dependent calmodulin [6]. While iNOS is a key mediator of inflammation and host defense systems, which expressed in macrophages induced by inflammatory stimuli such as interferon (IFN), tumor necrosis factor (TNF), and bacterial lipopolysaccharide (LPS) [7]. The overproduction of NO due to the prolonged induction of iNOS has been observed in chronic inflammatory diseases, asthma, septic shock and rheumatoid arthritis [8-10]. Thus, iNOS has become a potential target in the treatment of inflammatory and autoimmune diseases [11].

The whole plant of *Solanum cathayanum* has been widely used as a folk medicine for anti-inflammatory and antitumor treatment in China. Recently, compound **1** (8-hydroxy-3-methoxy-5H-pyrido [2, 1-c] pyrazin-5-one) (Fig. 1) was isolated from *Solanum cathayanum* by our group [12] and identified as a LPS-induced iNOS inhibitor with IC_{50} value 30 μM. To enhance the inhibition activity, compound **1** should be modified in the further work. Therefore, the objectives of this article were to investigate the interaction mechanism between compound **1** and iNOS by

induced-fit docking (IFD) method, and design the derivatives of compound **1** as novel iNOS inhibitors using combinatorial virtual screening technology.

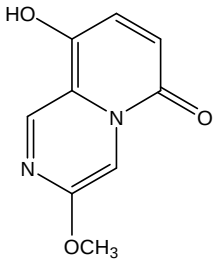

Fig. 1 Chemical structure of compound 1

EXPERIMENTAL SECTION

iNOS activity determination:

The iNOS inhibition activity of compound **1** was evaluated for the inhibition of NO production in LPS-activated murine macrophage (RAW 264.7 cells). The amounts of NO released into culture media were determined by the Griess method in the form of nitrite [13]. RAW 264.7 cells in 10% fetal bovine serum (FBS)-DMEM medium, were plated in 48-well plates (1×10^5 cells/mL), and then incubated for 24 h. The cells were replaced with fresh media with 1% FBS, and then incubated for 20 h in the presence or absence of test compounds with LPS (1 μg/mL). NO production in each well was assessed by measuring the accumulated nitrite in culture supernatant. Samples (100 μL) of media were incubated with Griess reagent (150 μL) for 10 min at room temperature in 96 well microplate. Absorbance at 540 nm was read with a microplate reader. A standard calibration curve was prepared using sodium nitrite as a standard. The results were typically expressed as IC_{50} value (the concentration of inhibitor to inhibit 50% activity).

Induced-fit docking:

Molecular docking simulation was performed using induced-fit docking (IFD) method [14] in the Schrödinger software suite [15], which had been reported to be a robust and accurate method to account for both ligand and receptor flexibility [16]. The atomic co-ordinates for the structure of iNOS were downloaded from the Protein Data Bank (PDB code: 3NQS, 2.2 Å resolution) [17]. The subsequent 3NQS model was subject to the Protein Preparation Wizard module in Schrödinger as follows: adding hydrogen, assigning partial charges using the OPLS-2001 force field, and assigning protonation states. All crystal waters were removed. Then the minimization was carried out using the OPLS force field in the MacroModel module in Schrödinger [15] with backbone atoms being fixed.

The IFD protocol was carried out in three consecutive steps [18, 19]. Firstly, the ligand was docked into a rigid receptor model with scaled-down van der Waals (vdW) radii. A vdW scaling of 0.5 was used for both the protein and ligand non-polar atoms. The Glide SP mode [20] was used for the initial docking, and 20 ligand poses were retained for protein structural refinements. The docking box was defined to include all amino acid residues within the dimensions of 20 Å × 20 Å × 20 Å from the center of the ligand (AT2) in 3NQS. Secondly, Prime program was used to generate the induced-fit protein–ligand complexes. Each of the 20 structures from the previous step was subjected to side chain and backbone refinements. All residues with at least one atom located within 5.0 Å of each corresponding ligand pose were included in the Prime refinement [21]. The refined complexes were ranked by Prime energy, and the receptor structures within 30 kcal/mol of the minimum energy structure were passed through for a final round of Glide docking and scoring. Finally, each ligand was redocked into every refined low-energy receptor structure produced in the second step using Glide SP mode at default settings. An IFD score (IFD score = 1.0 Glide_Gscore + 0.05 Prime_Energy) that accounts for both the protein–ligand interaction energy and the total energy of the system was calculated and used to rank the IFD poses. The more negative IFDscore, the more favorable the binding. The final ligand–protein complexes were visualized using PyMOL0.99 [22] and Ligand Interactions module embedded in Maestro 9.3 [23].

Combinatorial screening:

Combinatorial screening method [24] was used in virtual screening of the derivatives of compound **1** as iNOS inhibitors. The virtual screening flow is as follows:

(1) Combinations definition. To synthesize conveniently, the different substituted ethers were set by side- chain hopping in oxymethyl and hydroxyl sites of compound **1** (Fig. 2).

(2) Virtual combinatorial library generation. The reagent fragments (including R-O- group) were built from in-house drug-like database (5,680 compounds) and iteratively combined with the core of compound **1**. All possible combinations (about 32,160 virtual compounds) were produced and used as an input compound library for virtual screening.

(3) Virtual screening. The applied screening protocol consisted of three filtering phases: Firstly, Glide SP docking was performed to virtual compound library. Secondly, the Lipinski rules of five were applied to filter off compounds with unfavorable profiles. Thirdly, induced-fit docking was used to the top 50 compounds according to Gscore. The final top 5 compounds scored by IFD score were selected.

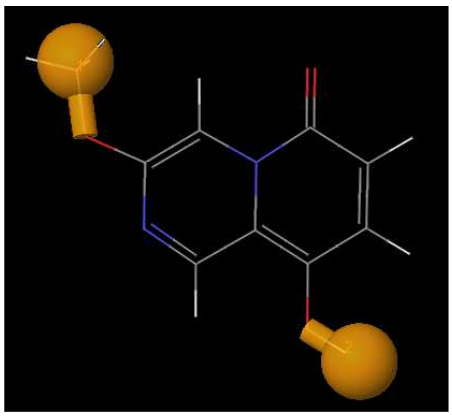

Fig. 2 The definition of compound combinations

RESULTS AND DISCUSSION

The validation of IFD model was performed before docking simulation. The superposition of the IFD-generated AT2 model (carbons in green, Fig. 3) to the native structure of AT2 (carbons in gray, Fig. 3) in AT2/iNOS complex (3NQS) yielded a RMSD of 0.15 Å for all heavy atoms (excluding the hydrogen atoms). Obviously, the IFD-generated AT2 model is very close to the native ligand in the crystal 3NQS. Hence, the IFD module could be applied to predict the binding interactions between inhibitors and iNOS.

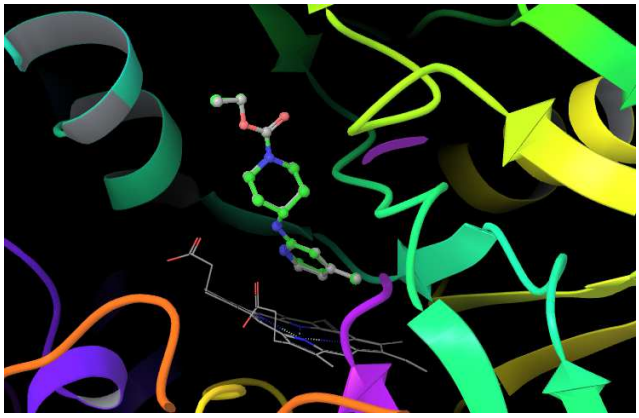

Fig. 3 The binding sites of 3NQS with AT2: native AT2 (gray carbons), IFD-generated AT2 model (green carbons)

Compound **1** is a potent iNOS inhibitor with IC_{50} value 30 μM. Induced-fit docking between compound **1** and iNOS was simulated. The Glide Gscore and IFD score of compound **1** (the best pose) are –6.99 and –766.90, while those of AT2 (IC_{50} =0.35 μM) are –7.02 and –768.47, respectively (Table 1). Based on the crystal structure of 3NQS, AT2

forms two strong hydrogen bonds with Tyr341 (the distance: 1.87 Å) and Glu371 (1.86 Å) (Fig. 4A; Table 2). Hydroxyl group of compound **1** in docking complex has hydrogen bond interaction (the distance: 1.72 Å) with cofactor Hem901 (iron protoporphyrin) (Fig. 4B; Table 2). Compound **1** and AT2 all show hydrophobic interactions with Pro344, Val 346, Phe363, Trp366, and Tyr367. Both of them interact with Glu371 through negative charged interaction and with Asn364 via polar interaction. But the binding sites of AT2 are more than those of compound **1** including Arg260, Gln257, Trp340, Tyr341, Ala345, Asp376, and Arg382. From the superposition of IFD-generated compound **1** and AT2 in iNOS (Fig. 5), we can speculate that the modification of side chain in compound **1** could enlarge the binding sites of the ligand and enhance its inhibition activity.

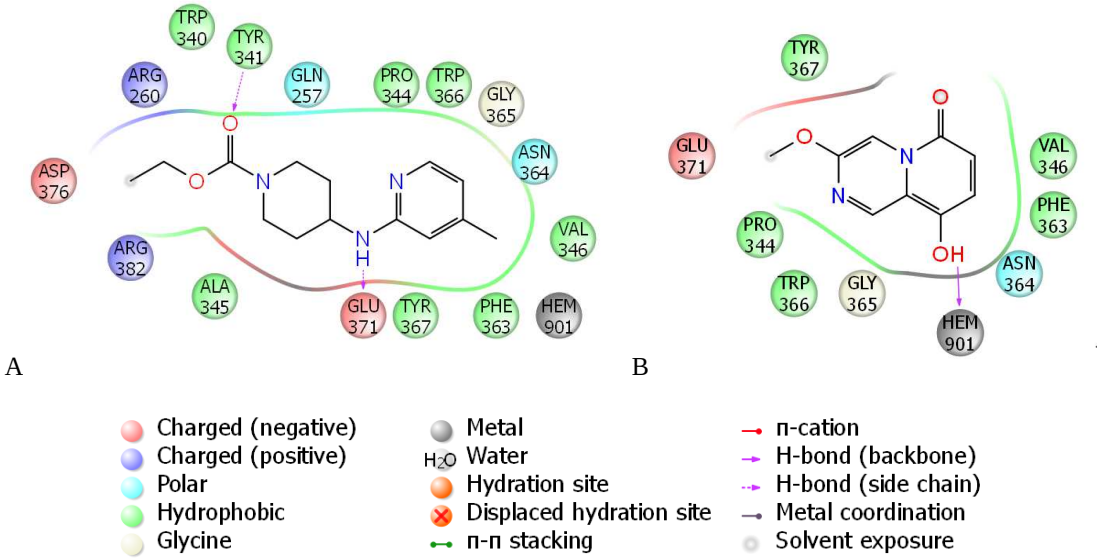

Fig. 4 The interaction modes of ligand with iNOS (3NQS): (A) AT2; (B) compound 1

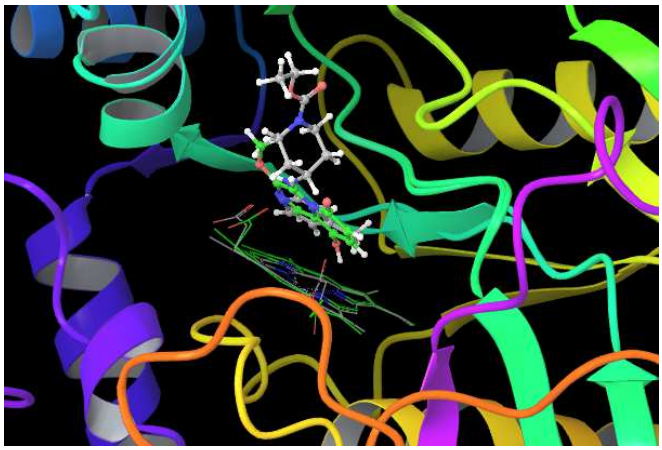

Fig. 5 The binding sites of iNOS (3NQS) with native AT2 (gray carbons) and IFD-generated compound 1 model (green carbons)

By virtual screening of the derivatives of compound **1**, the top 5 iNOS inhibitors were obtained. The structures and interaction modes of compounds are shown in Fig. 6. The Glide Gscores and IFD scores of top 5 compounds are all lower than AT2 (Table 1), which indicates that the selected derivatives of compound **1** would have higher iNOS inhibition activities than AT2 (IC_{50} <0.35 μM). To iNOS inhibitors, there are two interaction types: (1) type I, only interaction with residues in iNOS, including some important residues such as Gln257 [25], Tyr341 [26], Met368 [27], and Glu371 [28, 29]; (2) type II, interaction with both residues and iron protoporphyrin [4, 25, 30]. The selected derivatives of compound **1** belong to type II. Compound **2** (top 1, IFD score = –775.32) has strong hydrogen bonds with Asn348 (1.96 Å), Met368 (2.22 Å) and Hem901 (1.61 Å) (Fig. 6A, Table 2). The core of

compound **3** (top 2, IFD score = –775.08) interacts with residues Gln257, Tyr367, Arg375, and Asp376 by hydrogen bonds, while the side chain of compound **3** has π-cation and hydrogen bond interactions with Hem901 (Fig. 6B, Table 2). Compound **4** (top 3, IFD score = –773.19) has two hydrogen bonds with Gln257 and four hydrogen bonds with hem901 (Fig. 6C, Table 2). Glu371 interacts with hydrogen atoms of imino-groups in compound **5** (top 4, IFD score = –771.91) via hydrogen bonds (Fig. 6D, Table 2). Compound **5** also has hydrogen bond interactions with Tyr341 and Hem901, and π-cation interactions with Arg375 and Hem901. Besides Gln257, there are three hydrogen bonds between Hem901 and compound **6** (top 5, IFD score = –769.00) (Fig. 6E, Table 2). The hydroxyl groups of compound **1**, **3**-**6** all have hydrogen bonds with iNOS, especially with Hem901 (compound **1**, **4**-**6**). Compared with compound **1**, the top 5 compounds have more binding sites (Fig. 6), which could increase their activities through hydrogen bond, hydrophobic, polar and charged interactions.

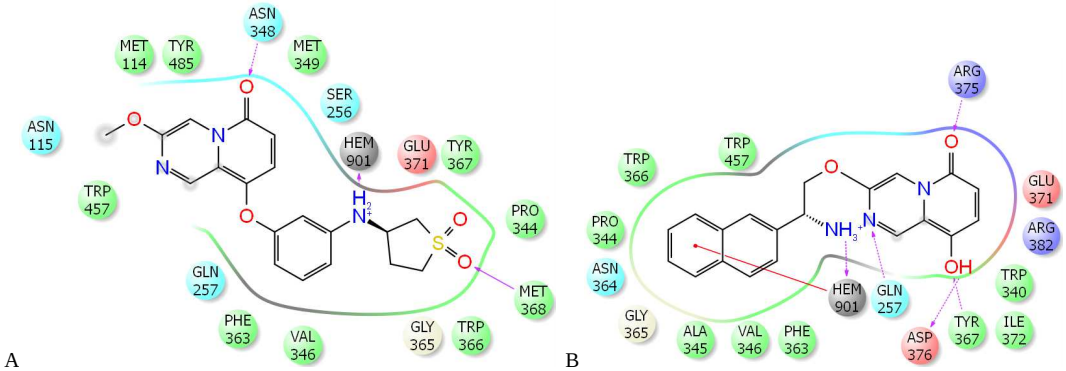

A B

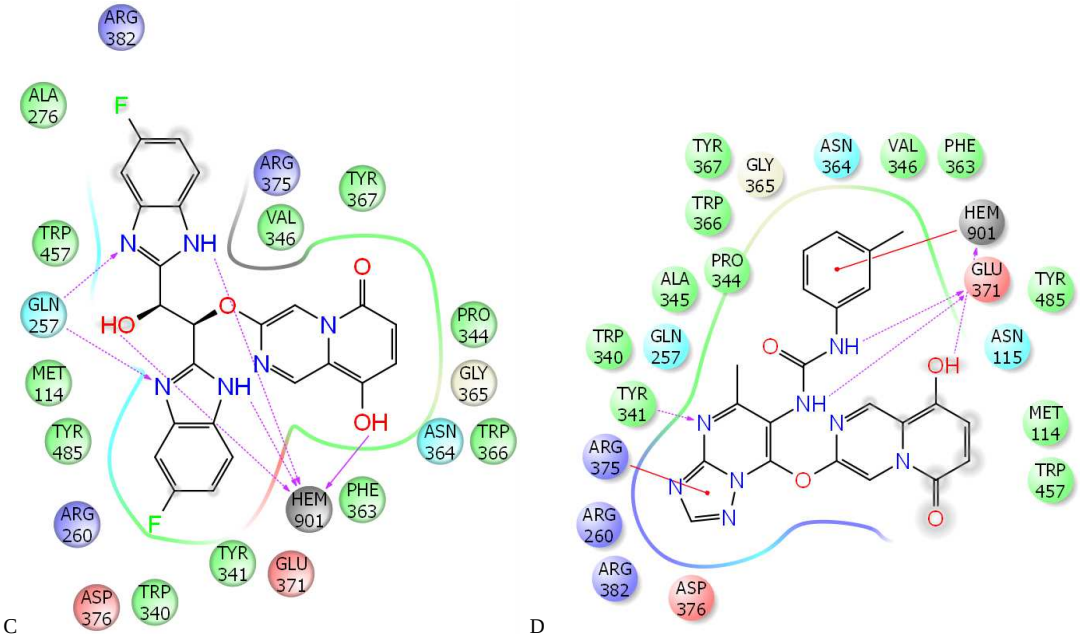

C D

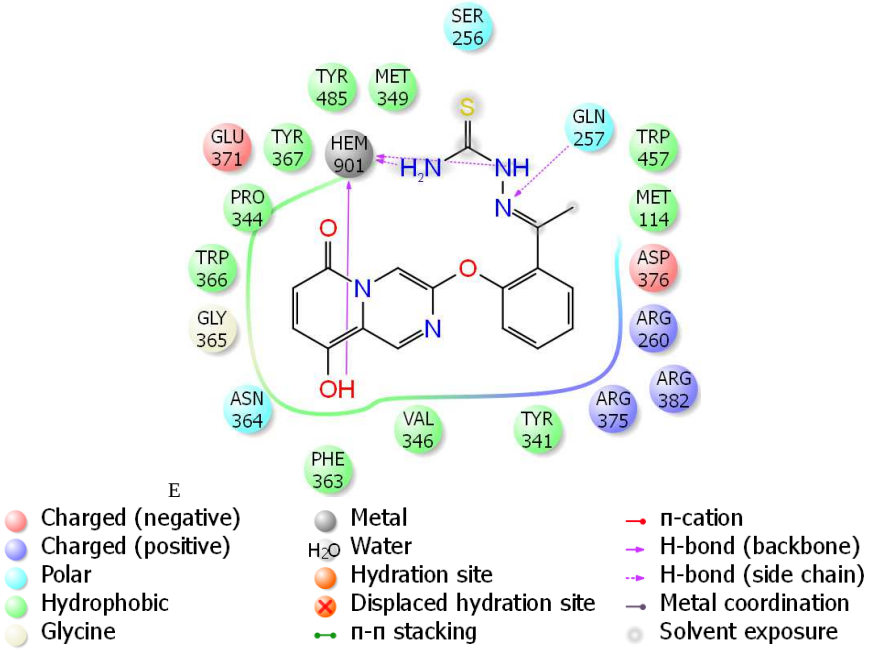

Fig. 6 The structures and interaction modes of top5 iNOS inhibitors: (A) compound 2 (top 1); (B) compound 3 (top 2); (C) compound 4 (top 3); (D) compound 5 (top 4); (E) compound 6 (top 5)

Table 1 The Glide Gscores and IFD scores of studied iNOS inhibitors

iNOS inhibitor	Gscore	IFD score
AT2	-7.02	-768.47
Compound **1**	-6.99	-766.90
Compound **2** (top 1)	-8.64	-775.32
Compound **3** (top 2)	-9.73	-775.08
Compound **4** (top 3)	-9.92	-773.19
Compound **5** (top 4)	-8.23	-771.91
Compound **6** (top 5)	-7.73	-769.00

Table 2 The hydrogen bond interactions between the ligands and residues of iNOS (3NQS)

Compounds	Atoms	Residues	Atoms	Distance(Å)
AT2	O16	Tyr341	HH	1.87
	HN8	Glu371	OE1	1.86
1	H5	Hem901	NC	1.72
2	O2	Asn348	HD22	1.96
	O4	Met368	H	2.22
	H11	Hem901	O1A	1.61
3	N1	Gln257	HE21	2.24
	O1	Tyr367	HH	1.94
	O2	Arg375	HH11	2.25
	H5	Asp376	OD2	1.98
	H7	Hem901	O1A	1.42
4	N3	Gln257	HE21	2.07
	N5	Gln257	HE22	2.39
	H5	Hem901	NC	2.14
	H10	Hem901	O1A	1.75
	H15	Hem901	O1A	1.80
	H16	Hem901	O1D	1.72
5	N5	Tyr341	HH	2.14
	H6	Glu371	OE1	2.42
	H7	Glu371	OE1	2.13
	H5	Hem901	O1D	1.78
6	N4	Gln257	HE21	2.43
	H5	Hem901	NC	2.20
	H6	Hem901	O1D	2.10
	H15	Hem901	O1D	1.68

CONCLUSION

Compound **1** (8-hydroxy-3-methoxy-5H-pyrido [2, 1-c] pyrazin-5-one) isolated from *Solanum cathayanum* was identified as a LPS-induced iNOS inhibitor with IC_{50} value 30 μM. The interaction mechanism between compound **1** and iNOS was investigated by induced-fit docking method. The Glide Gscore and IFD score of compound **1** are –6.99 and –766.90, respectively. Hydroxyl group of compound **1** has hydrogen bond interaction with cofactor Hem901. To enhance the inhibition activity, the derivatives of compound **1** were designed using combinatorial virtual screening technology. The IFD scores of top 5 compounds range from –769.00 to –775.32. The selected derivatives of compound **1** have more binding sites than compound **1**, and interact with both iron protoporphyrin and residues such as Gln257, Tyr341, Met368, and Glu371. The synthesis and activity evaluation of virtual screening compounds would be done in the future work.

Acknowledgments
This work was granted by National Natural Science Foundation of China (No. 30760213, 30870254) and Science Foundation of China Three Gorges University (No. KJ2010B001, 0620120052).

REFERENCES

[1] J MacMicking; QW Xie; C Nathan. *Annu. Rev. Immunol*., **1997**, 15, 323–350.
[2] T Michel; O Feron. *J. Clin. Invest*., **1997**, 100, 2146–2152.
[3] KA Hanafy; JS Krumenacker; F Murad. *Med. Sci. Monit.*, **2001**, 7, 801–819.
[4] BL Bourdonnec; LK Leister; CA Ajello; JA Cassel; PR Seida; HO Hare; M Gu; GH Chu; PA Tuthill; RN DeHavenb; RE Dolle. Bioorg. *Med. Chem. Lett*., **2008**, 18, 336–343.
[5] R Fedorov; E Hartmann; DK Ghosh; I Schlichting. *J. Biol. Chem*., **2003**, 278(46), 45818–45825.
[6] DK Ghosh; BR Crane; S Ghosh; D Wolan; R Gachhui; C Crooks; A Presta; JA Tainer; ED Getzoff; DJ Stuehr. *EMBO J*., **1999**, 18, 6260–6270.
[7] SP Singh; BK Konwar. *Springer Plus*, **2012**, 1, 69.
[8] C Bogdan. *Nat. Immunol*., **2001**, 2, 907–916.
[9] G Cirino; E Distrutti; JL Wallace. *Inflamm. Allergy Drug Targets*, **2006**, 5, 115–119.
[10] G Nagy; JM Clark; EI Buzas; CL Gorman; AP Cope. *Immunol. Lett*., **2007**, 111, 1–5.
[11] H Zhang; JH Zan; GY Yu; M Jiang; PX Liu. *Int. J. Mol. Sci*., **2012**, 13, 11210–11227.
[12] F Cheng; X Li; JZ Wang. *Chinese Chemical Letters*, **2008**, 19, 68–70.
[13] JY Kim; SJ Park; KJ Yun; YW Cho; HJ Park; KT Lee. *Eur. J. Pharmacol*., **2008**, 584, 175–184.
[14] W Sherman; T Day; MP Jacobson; RA Friesner; R Farid. *J. Med. Chem*., **2006**, 49, 534–553.
[15] Schrödinger, LLC, New York, NY, **2010**, www.schrodinger.com
[16] H Zhong; LM Tran; JL Stang. *J. Mol. Graph. Model*, **2009**, 28, 336–346.
[17] RJ Rosenfeld; J Bonaventura; BR Szymczyna; MJ MacCoss; AS Arvai; JR Yates; JA Tainer; ED Getzoff. *J. Biol. Chem*., **2010**, 285(41), 31581–31589.
[18] H Wanga; R Aslanian; VS Madison. *J. Mol. Graph. Model*, **2008**, 27, 512–521.
[19] HJ Luo; JZ Wang; WQ Deng; K Zou. *Med. Chem. Res*., **2013**, 22, 4970–4979.
[20] RA Friesner; JL Banks; RB Murphy; TA Halgren; JJ Klicic; DT Mainz; MP Repasky; EH Knoll; M Shelley; JK Perry; DE Shaw; P Francis; PS Shenkin. *J. Med. Chem*., **2004**, 47, 1739–1749.
[21] MP Jacobson; DL Pincus; CS Rapp; TJF Day; B Honig; DE Shaw; RA Friesner. *Proteins*, **2004**, 55, 351–367.
[22] WL De Lano. DeLano Scientific LLC, San Carlos, CA, **2004**, http://pymol.sourceforge.net
[23] Maestro, version 9.3, Schrödinger, LLC, New York, NY, **2012**, www.schrodinger.com
[24] CombiGlide, version 2.6, Schrödinger, LLC, New York, NY, **2010**, www.schrodinger.com
[25] DD Davey; M Adler; D Arnaia; K Eagen; S Erickson; W Guilford; M Kenrick; MM Morrissey; M Ohimeyer; G Pan; VM Paradkar; J Parkinson; M Polokoff; K Salonz; C Santos; B Subramanyam; R Vergona; RG Wei; M Whitlow; B Ye; ZS Zhao; JJ Devlin; G Phillips. *J. Med. Chem*., **2007**, 50, 1146–1157.
[26] ED Garcin; AS Arvai; RJ Rosenfeld; MD Kroeger; BR Crane; G Andersson; G Andrews; PJ Hamley; PR Mallinder; DJ Nicholls; SA St-Gallay; AC Tinker; NP Gensmantel; A Mete; DR Cheshire; S Connolly; DJ Stuehr; A Aberg; AV Wallace; JA Tainer; ED Getzoff. *Nat. Chem. Biol*., **2008**, 4, 700-707.
[27] SA Jackson; S Sahni; L Lee; Y Luo; TR Nieduzak; G Liang; Y Chiang; N Collar; D Fink; W He; A Laoui; J Merrill; R Boffey; P Crackett; B Rees; M Wong; JP Guilloteau; M Mathieu; SS Rebello. *Bioorg. Med. Chem*., **2005**, 13, 2723.

[28] U Graedler; T Fuchss; WR Ulrich; R Boer; A Strub; C Hesslinger; C Anezo; K Diederichs; A Zaliani. *Bioorg. Med. Chem. Lett.*, **2011**, 21, 4228-4232.
[29] BR Crane; AS Arvai; R Gachhui; C Wu; DK Ghosh; ED Getzoff; DJ Stuehr; JA Tainer. *Science*, **1997**, 278, 425–431.
[30] HA Stefani; K Gueogjan; F Manarin; SHP Farsky; J Zukerman-Schpector; I Caracelli; SRP Rodrigues; MN Muscará; SA Teixeira; JR Santin; ID Machado; SM Bolonheis; R Curi; MA Vinolo. *Eur. J. Med. Chem*., **2012**, 58, 117–127.